



# Imaging black holes and jets with a VLBI array including multiple space-based telescopes

Vincent L. Fish<sup>a,\*</sup>, Maura Shea<sup>a,b</sup>, Kazunori Akiyama<sup>a,c</sup>

<sup>a</sup> *Massachusetts Institute of Technology, Haystack Observatory, 99 Millstone Hill Road, Westford, MA 01886, USA*

<sup>b</sup> *Wellesley College, Whitin Observatory, Wellesley, MA 02482, USA*

<sup>c</sup> *National Radio Astronomy Observatory Jansky Fellow, USA*

Received 17 December 2018; received in revised form 13 March 2019; accepted 20 March 2019

Available online 3 April 2019

## Abstract

Very long baseline interferometry (VLBI) from the ground at millimeter wavelengths can resolve the black hole shadow around two supermassive black holes, Sagittarius A\* and M87. The addition of modest telescopes in space would allow the combined array to produce higher-resolution, higher-fidelity images of these and other sources. This paper explores the potential benefits of adding orbital elements to the Event Horizon Telescope. We reconstruct model images using simulated data from arrays including telescopes in different orbits. We find that an array including one telescope near geostationary orbit and one in a high-inclination medium Earth of geosynchronous orbit can successfully produce high-fidelity images capable of resolving shadows as small as  $3 \mu\text{as}$  in diameter. One such key source, the Sombrero Galaxy, may be important to address questions regarding why some black holes launch powerful jets while others do not. Meanwhile, higher-resolution imaging of the substructure of M87 may clarify how jets are launched in the first place. The extra resolution provided by space VLBI will also improve studies of the collimation of jets from active galactic nuclei.

© 2019 Published by Elsevier Ltd on behalf of COSPAR.

**Keywords:** Galaxies; jets; Techniques: high angular resolution; Techniques: interferometric; Quasars: supermassive black holes

## 1. Introduction

The angular resolution of an interferometric baseline is approximately the observing wavelength divided by the baseline length  $\lambda/B$ . The choice of observing wavelength is often fixed by source properties, and in any case atmospheric absorption imposes site-dependent limits on what is possible. Many terrestrial arrays using very long baseline interferometry (VLBI), such as the Very Long Baseline Array (VLBA) or the Event Horizon Telescope (EHT), achieve high angular resolution by having telescopes that are thousands of kilometers apart. Here too, the size of the Earth imposes fundamental limits on the longest achievable baseline from the ground.

Longer baselines are achievable with space-borne elements. Space VLBI has successfully been accomplished at centimeter wavelengths with the Tracking and Data Relay Satellite System (TDRSS; [Levy et al., 1986](#)), Highly Advance Laboratory for Communications and Astronomy (HALCA) VLBI Space Observatory Programme (VSOP; [Hirabayashi et al., 1998](#)), and RadioAstron ([Kardashev et al., 2013](#)). Arrays with two space-borne elements have been proposed before at frequencies up to 43 GHz and 86 GHz ([Hong et al., 2014](#); [Murphy et al., 2005](#)).

The EHT is a millimeter-wavelength VLBI array whose primary goal is to image nearby supermassive black holes and jets of active galactic nuclei (AGNs). Currently observing at  $\lambda = 1.3 \text{ mm}$  (230 GHz), the fringe spacing ( $\lambda/B$ , where  $B$  is the projected baseline length) of the longest baselines correspond to an angular resolution  $\lesssim 25 \mu\text{as}$ , which is sufficient to resolve the shadow of the supermas-

\* Corresponding author.

E-mail address: [vfish@haystack.mit.edu](mailto:vfish@haystack.mit.edu) (V.L. Fish).

sive black holes of Sagittarius A\* and M87. The EHT is currently upgrading telescopes to perform VLBI at  $\lambda = 0.87$  mm (345 GHz), which will further improve angular resolution by a factor of 1.5.

The EHT has developed imaging algorithms to produce superresolved images to make the most out of its data (e.g., Bouman et al., 2016; Chael et al., 2016; Akiyama et al., 2017a,b; Kuramochi et al., 2018). Nevertheless, the EHT is up against some hard limits. The Earth's atmosphere quickly becomes unsuitable for ground-based VLBI at higher frequencies, and existing baselines already approach an Earth diameter. In order to achieve higher angular resolution, it will be necessary to incorporate space-borne elements into VLBI arrays of the future.

Adding space-borne antennas to the EHT opens up new science that is very difficult or impossible from the ground. Reconstructing reliable movies of Sgr A\* is likely to require fast  $(u, v)$  coverage not currently obtainable from Earth-rotation aperture synthesis<sup>1</sup> (Palumbo et al., 2018). The ability to resolve and image fine-scale structures (smaller than the gravitational radius,  $r_g = GM/c^2$ ) in the flow around M87 will help enormously in understanding the details of how jets are launched. Adding to the EHT one or more telescopes near geosynchronous orbit would enable detailed study of other black hole sources such as the Sombrero Galaxy, an M87 analogue with a much weaker jet. Space VLBI will also help answer the question of whether jet collimation is universal across a wide range of jet power. And, as is clear from the diversity of presentations at the workshop “The Future of High-Resolution Radio Interferometry in Space” held in Noordwijk, The Netherlands, in 2018,<sup>2</sup> AGN jet science is just one of the many areas where space VLBI could have a large impact.

In this work, we focus on the applicability of a 230 GHz space-VLBI array to AGN jet studies. We motivate an architecture and possible space-VLBI array from practical considerations (Section 2), generate synthetic data (Section 3), and examine the imaging power of such an array (Section 4). We find that an array consisting of a half dozen or so satellites of modest aperture can provide the fast microarcsecond-scale angular resolution needed to make next-generation breakthroughs in AGN jet science.

## 2. Considerations for designing a space VLBI array

### 2.1. Technical assumptions

This work focuses on what could be achieved scientifically by launching highly capable satellites into several

classes of orbits around the Earth. Issues regarding technology and engineering are necessarily beyond the scope of this work, and in any case it is impossible to predict with full accuracy what the landscape will look like in the future. Nevertheless, it is worth specifying a few key technical assumptions to assess whether the concept described in this paper might be feasible within the next 5–10 years.

The cost of access to space is decreasing. Rideshare opportunities are becoming plentiful, with reduced or even zero marginal launch costs for secondary payloads. Taking full advantage of these opportunities will likely require that space-VLBI payloads fit within the size and weight limits of a small satellite that could be launched from an EELV (Evolved Expendable Launch Vehicles) Secondary Payload Adapter (ESPA) Grande ring, for instance. As an added benefit, keeping the payload size small may reduce the cost per satellite, potentially allowing for more satellites to be built and launched. A rideshare strategy argues for choosing classes of orbits with frequent launches (e.g., LEO and GEO) rather than requiring bespoke orbital parameters.

Our vision assumes improvements in some space-borne telescope subsystems that we believe to be tractable within less than a decade. We assume that an aperture of a few meters in diameter with appropriate surface accuracy for observations at 1.3 mm can be deployed cheaply. One promising approach might be to stow the surface within a standard secondary payload volume and unfurl it in space. Other approaches may become financially viable as the increasing number of commercial launch opportunities drive costs down. We assume that stable receivers and signal chains with bandwidths of many GHz can provide adequate sensitivity at a cost that is not prohibitive. We assume that a very accurate frequency standard can be provided at reasonable cost. Onboard atomic clocks on each element may be the easiest solution, although distributed signals with a round-trip loop may also be feasible. We assume that laser communications links will be able to support data rates of many gigabits per second. Transferring large amounts of data to the ground may require substantial onboard data storage and a geosynchronous satellite acting as a relay.

We have been purposefully vague in the preceding paragraph. Other scientific, industrial, and military applications are already driving some of the assumed advances. Given adequate time and funding, focused efforts could enable major progress in the remaining areas. All of the required pieces of technology for a space-VLBI 1.3 mm array exist, even if cost or performance issues may preclude advancing a complete mission today. Furthermore, as will become clearer in Section 2.5, the achievable performance of a space-VLBI array depends on multiple parameters (aperture size, aperture efficiency, bandwidth, and system temperature) of both the space-based and ground-based elements. Improvements in one of these parameters are interchangeable with improvements in another.

<sup>1</sup> It is possible that a large number of additional ground stations could enable snapshot imaging of Sgr A\*, although the geographical distribution of sites suitable for 230 GHz observing imposes fundamental limits on a ground-only approach.

<sup>2</sup> <https://www.ru.nl/astrophysics/news-agenda/future-high-resolution-radio-interferometry-space/submitted-abstracts/> (accessed 2019 March 13).

## 2.2. Timescales

In order to produce static images or movies of a source with varying structure, it is desirable to sample the  $(u, v)$  plane before the source structure changes appreciably. A useful characteristic timescale for a black hole source is  $t_g = GM/c^3$ , the light-crossing time of the gravitational radius. For Sgr A\*, whose mass is approximately  $4.3 \times 10^6 M_\odot$ , this time is about 20 s. Structures in an accretion flow may be bigger than  $r_g$ , and material in the accretion flow moves at subluminal velocities, so a source may effectively be static over a timescale of a few  $t_g$ . Indeed, Sgr A\* is seen to vary across the electromagnetic spectrum on timescales of minutes (e.g., Marrone et al., 2008).

Other supermassive black holes of interest are much more massive and therefore vary on longer timescales. For instance,  $t_g \approx 9$  hr for M87, assuming a mass of  $6.6 \times 10^9 M_\odot$  (Gebhardt et al., 2011). For these sources, visibilities obtained over the course of a day are sampling a nearly static source.

For more distant sources, structural changes are only relevant if they are on a sufficiently large angular scale to be detected. AGN jets often exhibit superluminal apparent motion, but these sources are farther away, resulting in a small apparent angular motion on the sky. For instance, features in the jet of 3C 279 are seen to move at many times the speed of light (Whitney et al., 1971; Kellermann et al., 1974; Cohen et al., 1977, and many others), corresponding to a motion of  $1 \mu\text{as}$  in a few days. Such structural changes are evident in early EHT data, which detected small changes in the closure phase even on a triangle of stations with a longest baseline of 3–4  $G\lambda$  (Lu et al., 2013). The fractional changes in the data on longer (e.g., space-ground) baselines would, of course, be substantially larger.

It is possible for small portions of a source to vary in brightness on even faster timescales. In this case, it may be possible to mitigate the loss in image fidelity by treating the constant and variable components separately when calibrating the data, as is sometimes done for connected-element interferometry of Sgr A\* (e.g., Marrone et al., 2007, 2008).

Thus, with the exception of Sgr A\*, nearly all supermassive black hole targets of a millimeter-wavelength space-VLBI array can be considered to be static on the timescale of a day. The orbits of the satellites in a millimeter-wavelength space-VLBI array should therefore be designed to swing through  $(u, v)$  space on timescales of approximately one day or less. This argues for the highest element of an Earth-centered space-VLBI array to be near geosynchronous orbit.

## 2.3. Baseline coverage

All things being equal, a VLBI array with smaller coverage holes in the  $(u, v)$  plane will produce images with higher fidelity, since there are fewer missing data points for image

reconstruction algorithms to have to try to fill in. The finer angular resolution provided by very long baselines is desirable, but it can be difficult or impossible to reconstruct images from long-baseline data without data on short and intermediate baselines to fill in the gaps. This argues against placing a single satellite in a very high orbit.

The short baselines will be especially important in all but the most compact sources. A baseline of  $1D_\oplus$  is approximately  $10 G\lambda$  at  $\lambda = 1.3$  mm, with a fringe spacing of  $\lambda/D \approx 20 \mu\text{as}$ . Almost all AGN jet sources have structure on scales larger than this, sometimes into the hundreds or thousands of microarcseconds in extent. Short ( $< 1D_\oplus$ ) baselines to reconstruct the large-scale emission will be necessary to make use of longer baselines for the increased angular resolution. This argues for the inclusion of either ground-ground VLBI baselines or enough elements in low Earth orbit (LEO) to fill in the center of the  $(u, v)$  plane.

Sky images are inherently two-dimensional. Previous space-VLBI efforts have focused on placing a single element into orbit (Levy et al., 1986; Hirabayashi et al., 1998; Kardashev et al., 2013). RadioAstron provides an instructive case: its images often suffer from having poor resolution orthogonal to the direction of its orbit (e.g., Gómez et al., 2016). An imaging array should therefore have at least two elements in high, approximately orthogonal orbits.

## 2.4. Classes of orbits

Low Earth orbits range from a few hundred to 2000 km above the ground. Since the mean radius of the Earth is approximately 6370 km, satellites in LEO do not significantly extend angular resolution beyond what is available from a ground-based array alone. However, LEO orbits provide fast baseline coverage. Satellites in LEO circle the Earth in approximately 90 to 120 min. LEO-ground and LEO-LEO baselines can quickly fill in the  $(u, v)$  plane out to  $\sim 12 G\lambda$  at 1.3 mm. Even for “snapshot” observations of a few minutes, during which ground-ground baselines are effectively stationary in the  $(u, v)$  plane, LEO-ground baselines sweep out substantial arcs. Satellites in LEO may therefore be essential for dynamic imaging of Sgr A\* (Palumbo et al., 2018). Satellites in LEO are also helpful for fast imaging of M87, though they are not as critical as for Sgr A\*, due to the longer timescale of variability in M87 (Section 2.2).

With orbits at  $\sim 6.6R_\oplus$ , satellites in geosynchronous Earth orbit (GEO) provide significantly more angular resolution than LEO. More than one satellite near GEO or Medium Earth orbit (MEO) may be required in order to provide approximately equal angular resolution at a wide range of position angles on the sky. A GEO satellite could serve double duty as the communications link to other satellites in the array. Satellites in LEO are only visible from a ground station for a small fraction of their orbit, yet for most of their orbit they have a direct line of sight

to a geosynchronous satellite, which in turn is always visible from the ground.

Higher orbits provide even greater angular resolution at the expense of slower  $(u, v)$  coverage. Very high orbits (e.g., translunar or Sun–Earth L2) may provide insufficient  $(u, v)$  coverage to produce a high-fidelity image within the time-scale of variation of many sources, with the additional problem that the lack of intermediate-length baselines would make it very difficult to connect data from the remote space-borne element to the ground array (or satellites near the Earth). Therefore, for the remainder of this work we consider space arrays consisting only of telescopes in GEO or lower: GEO or high MEO satellites for angular resolution, LEO satellites for fast baseline coverage (for snapshot imaging of Sgr A\*) or dense sampling of baselines within about an Earth diameter (for higher image fidelity of other sources), and ground-based telescopes for sensitivity.

### 2.5. Aperture and sensitivity

It can be expensive to build and launch large apertures. Rocket payload fairings will impose a maximum upper size to potential satellites. While we cannot predict at this time what this size will be many years in the future, it seems prudent to try to limit the aperture size to a few meters in diameter.

The system equivalent flux density (SEFD) of a telescope is related to the geometric area ( $A$ ), aperture efficiency ( $\eta_A$ ), and the system temperature ( $T_{\text{sys}}$ ) by

$$\text{SEFD} = \frac{2kT_{\text{sys}}}{\eta_A A} \approx 42000 \text{Jy} \left( \frac{D}{3\text{m}} \right)^{-2} \left( \frac{\eta_A}{0.7} \right)^{-1} \left( \frac{T_{\text{sys}}}{75\text{K}} \right), \quad (1)$$

with lower values corresponding to more sensitive telescopes. As a point of reference, the system temperature of the Atacama Large Millimeter/submillimeter Array (ALMA) is approximately 75 K in the lower part of the 230 GHz band in very dry conditions (Warmels et al., 2018). While all current ground-based observatories in the EHT are capable of producing a lower SEFD at high elevation in good weather, some EHT scans in 2013 with the Submillimeter Telescope (SMT) in Arizona or a single Combined Array for Research in Millimeter-wave Astronomy (CARMA) dish in California had SEFDs near or above 42000 Jy on Sgr A\* due to a combination of mediocre weather and low source elevation (Johnson et al., 2015). A satellite of modest aperture can achieve the sensitivity of a significantly larger aperture on the ground.

The sensitivity of a baseline of two telescopes is given by

$$\sigma = \frac{1}{\eta_Q} \sqrt{\frac{\text{SEFD}_1 \text{SEFD}_2}{2\Delta\nu\tau}}, \quad (2)$$

where  $\sigma$  is the noise,  $\eta_Q$  is the sampling quantization loss factor ( $\sim 0.88$  for 2-bit sampling),  $\Delta\nu$  is the bandwidth, and  $\tau$  is the integration time. Thus, all else being equal, the rms noise on a space–ground baseline scales as

$$\sigma \propto (A_{\text{space}} A_{\text{ground}} \Delta\nu\tau)^{-1/2}, \quad (3)$$

where  $A$  is the area of each aperture. This immediately suggests that a cost-effective strategy to achieve high sensitivity is to build modest space apertures that leverage the very sensitive apertures on the ground and to observe with a high bandwidth. If the partner station is phased ALMA with an SEFD of 70 Jy (Fish et al., 2013) and an observing bandwidth of 8 GHz,  $\sigma \approx 2$  mJy in one minute to a 42000 Jy space telescope. Even wider bandwidths are possible from ground-based telescopes, as demonstrated by the upgraded Submillimeter Array (SMA) system (Primiani et al., 2016).

These bandwidths are significantly larger than used by previous space VLBI efforts. VSOP and RadioAstron both typically observe(d) two 16 MHz channels for a total data rate of 128–144 Mbs<sup>-1</sup>, transmitted back to the ground at radio frequencies (Hirabayashi et al., 1998; Kardashev et al., 2013). Both of these missions were designed in an era when this was a typical data rate for terrestrial VLBI.

There are many sensitive ground stations, including phased ALMA, the Large Millimeter Telescope (LMT) Alfonso Serrano in Mexico, the phased SMA in Hawai'i, and the phased Northern Extended Millimeter Array (NOEMA) in France. Any one of these would be likely be sufficient to obtain rapid detections to a space aperture. So long as fringes can be found to all telescopes from a sensitive ground station, data on all baselines can be fringe fitted and used, even if the instantaneous signal-to-noise ratio (SNR) is small in any given interval.

## 3. Methods

### 3.1. General approach

Current studies have created arrays with space-based telescopes that are designed for one particular purpose. For instance, Palumbo (2018) explored an array consisting of four telescopes in LEO, optimized for dynamical imaging. Roelofs et al. (submitted for publication) explored a minimal configuration of two MEO satellites in a configuration such that the orbits slowly evolve over the course of six months to image Sgr A\*. The uniting theme in these studies is that they have focused on a single scientific case and identified a single type of array to address that specific case. In this paper, we focus on an array configuration that can flexibly address multiple science cases.

Building off of the concept of Palumbo (2018), we start with a LEO array consisting of up to four telescopes, which provides excellent  $(u, v)$  coverage within  $\sim 10 G\lambda$  at 230 GHz. We add a geosynchronous satellite to significantly increase the resolution in the east-west direction. This single satellite can also provide north-south coverage for high-declination sources. To add north-south coverage for the rest of the sky, we add a satellite in an inclined, eccentric MEO orbit. Given these constraints, we have chosen satellites from among existing unclassified NORAD two-line

elements (TLEs) available from CelesTrak<sup>3</sup> in order to simulate data from satellites in real orbits. The selection of these satellites is quasi-arbitrary, and our results do not appear to be particularly dependent upon the specific satellites chosen, which is encouraging for a rideshare concept. A more detailed trade study of orbital parameters would, of course, be necessary before a specific mission is advanced.

### 3.2. Imaging

Representative model images were selected, and then simulated data were produced using the `ehtim` (`eht-imaging`) library. The ground array was assumed to include the observatories that currently observe as part of the EHT: ALMA, the Atacama Pathfinder Experiment (APEX), the Greenland Telescope (GLT), the James Clark Maxwell Telescope (JCMT), the LMT, the IRAM 30-meter telescope on Pico Veleta, the South Pole Telescope (SPT), the SMA, and the SMT. Other ground observatories, NOEMA and the ALMA prototype antenna at Kitt Peak, are currently being upgraded to join the EHT and were therefore included as well.

To reduce the number of data points to be imaged (thereby speeding convergence), we simulate data with  $\tau = 360$  s and  $B = 4$  GHz over a 24-h period. From Eq. (3), this is equivalent to  $\tau = 90$  s with two orthogonal polarizations, each of  $B = 8$  GHz. Large integration times limit the field of view that can be imaged, although data can be segmented to much shorter time intervals after fringes are found. Data with SNR less than 3 were flagged.

Fig. 1 illustrates a representative  $(u, v)$  coverage that the space array might obtain. The baselines involving at least one ground station (red, black, and blue points) have enough sensitivity to be able to detect sources with as little as a few mJy of correlated flux density. For weak sources, the space–space baselines (green points) may fall below the SNR cutoff for useful data. Regardless, the space–space baselines add little  $(u, v)$  coverage that cannot be obtained from space–ground baselines alone.<sup>4</sup>

Datasets to image consisted of visibility amplitudes and closure phases. For ground-based stations, absolute visibility phases are difficult to estimate due to very rapid variations in tropospheric delays. Space–space baseline phases will be uncontaminated by these atmospheric contributions, and it is possible that visibility phases will be usable on these baselines directly, along with hybrid mapping techniques to estimate visibility phases on other baselines. Nevertheless, for simplicity our reconstructions use closure phases as the only phase information included.

Images were then reconstructed from the simulated data using the Sparse Modeling Imaging Library for Interferometry (SMILI). In addition to incorporating a sparsity ( $\ell_1$ -norm minimizing) regularizer, SMILI includes total variation (TV) and total square variation (TSV) regularizers for smoothness (Akiyama et al., 2017b; Kuramochi et al., 2018). In our simulations, we use both the sparsity and TSV regularizers. Optimal values of the hyperparameters are determined using a cross-validation approach on a ground-truth data set. Images were reconstructed from three arrays: a ground-only array (i.e., without any elements in space), a ground + LEO array, and a full array consisting of the ground + LEO array plus one satellite each in equatorial GEO and high-inclination MEO.

## 4. Results

To demonstrate the power of a full space-VLBI array, we examine three scientific use cases relevant to supermassive black holes and AGN jets. Can a full space array resolve the black hole shadow in sources other than Sgr A\* and M87, and, if so, what is the limit? Can such an array resolve details of the jet launch zone of M87? And can it bring out the fine details necessary to help understand the collimation and propagation of AGN jets?

### 4.1. Resolving shadows around other black holes

The two prime targets of the EHT, Sgr A\* and M87, are the only known black hole sources for which terrestrial VLBI at 1.3 mm can resolve the shadow around the black hole. The increased resolution of space VLBI can extend this capability to new sources.

Johannsen et al. (2012) originally looked at prospects for obtaining masses of other nearby supermassive black holes using VLBI. One of the most promising sources on their list is the Sombrero Galaxy (NGC 4594, M104). The supermassive black hole in M104 has a mass of  $6.6 \times 10^8 M_{\odot}$  at a distance of 9.9 Mpc (Greene et al., 2016), which leads to a predicted shadow diameter of  $\sim 6.8 \mu\text{as}$ . At longer wavelengths, the emission is seen to be very compact, with a slight elongation indicating the presence of a very weak jet (Hada et al., 2013). The authors contrast M104 with M87, which has a much more powerful radio jet, and note the importance of observing M104 at high angular resolution to determine whether the stark difference in jet power is due to differences in the black hole spin, the accretion rate, or other properties of the accretion flow, going so far as to say that “M104 and M87 are a unique pair for testing this issue because the black hole vicinity is actually accessible at a similar horizon-scale resolution.”

Fig. 2 illustrates the importance of having telescopes in MEO or GEO orbits to image the black hole region of the Sombrero Galaxy. Neither the ground array alone nor an array consisting of both ground and LEO telescopes is suf-

<sup>3</sup> satellite numbers 07276, 19822, 25635, 27854, 29107, and 43132 from <https://www.celestrak.com/NORAD/elements>.

<sup>4</sup> A possibly significant exception to this is the baseline between the two MEO/GEO satellites, which samples a different area of  $(u, v)$  space. This baseline vector changes very slowly, and it may be possible to integrate for  $\tau \gg$  several minutes to obtain robust detections.

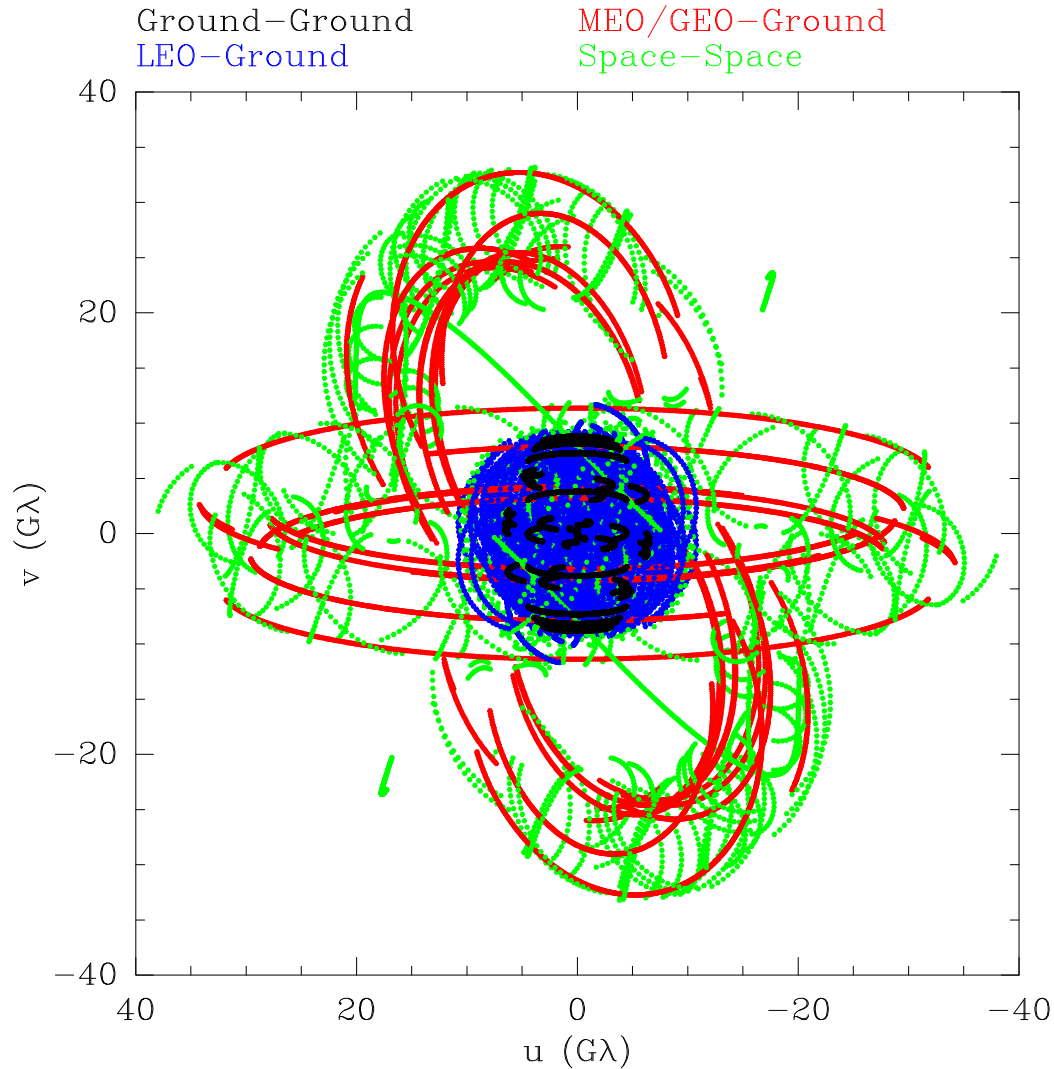


Fig. 1. Representative  $(u, v)$  coverage obtainable in 24 h for a source at the declination of M104. Individual points are spaced 90 s apart. The addition of telescopes in MEO/GEO significantly expands the maximum baseline length compared to LEO alone.

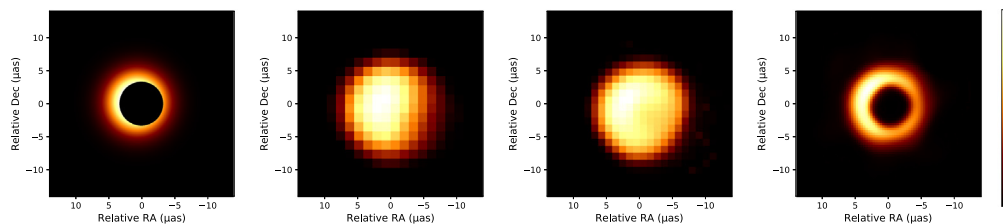


Fig. 2. Imaging simulation of the Sombrero Galaxy. *Left to right*: Model image, reconstruction with the ground array only, with the ground array plus four telescopes in LEO, and with the full space array. The shadow region can be resolved, but only if telescopes in MEO/GEO orbits are included. A linear transfer function from zero to the maximum pixel value, as shown in the colorbar on the right, is used in this and the two subsequent figures. Pixel sizes are automatically selected based on the effective resolution of the array. (For interpretation of the references to colour in this figure legend, the reader is referred to the web version of this article.)

ficient to resolve the black hole shadow region. The shadow is well imaged when MEO/GEO satellites are included. (We have assumed a static image for these simulations, but several tracks may be required if the source is in an active state, since  $t_g$  is about an hour for the Sombrero

Galaxy.) Simulations demonstrate that the full space array could resolve a black hole shadow down to approximately  $3 \mu\text{s}$  in diameter (Fig. 3), which would add M104, IC 1459, M84, and perhaps IC 4296 to the list of supermassive black holes that are bright enough and are predicted to have a

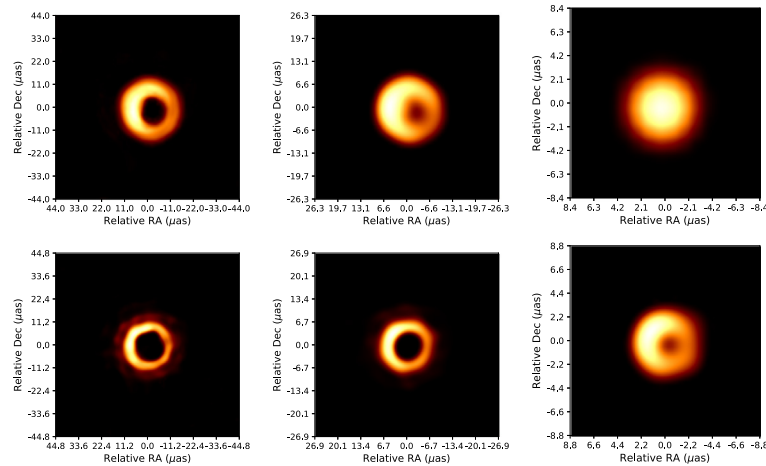


Fig. 3. Test to determine the shadow resolution power of space arrays. In the panels from left to right, the model (left panel of Fig. 2) was rescaled to have a shadow diameter of  $15 \mu\text{as}$ ,  $9 \mu\text{as}$ , and  $3 \mu\text{as}$ . The top row shows reconstructions from the ground + LEO array, which can marginally resolve shadows down to a diameter of  $9 \mu\text{as}$ . The bottom row shows reconstructions from the full space array, which can marginally resolve shadows down to  $3 \mu\text{as}$ .

sufficiently large shadow to be resolved<sup>5</sup> (see Johannsen et al., 2012 for mass and distance estimates).

#### 4.2. M87 jet launch

The shadow of M87 is within the reach of the resolution of a ground-based array alone, and it is probable that the EHT will produce successful images of the M87 shadow within the next few years. Models of M87 suggest that the 1.3 mm emission is mainly concentrated near the shadow region (e.g., Broderick and Loeb, 2009; Dexter et al., 2012; Mościbrodzka et al., 2016), a conclusion supported by early EHT data (Doeleman et al., 2012). In contrast, longer-wavelength data show a prominent jet extending far away from the location of the black hole (e.g., Walker et al., 2018). How this jet is launched is an open question.

Inhomogeneities in the accretion disk and jet may produce useful tracers of the motions and magnetic field in the jet launch region around the black hole. The models of Mościbrodzka et al. (2016, 2017) illustrate physically plausible emission profiles that might be seen at millimeter wavelengths. Imaging and tracking the evolution of these substructures may help to distinguish whether the observed emission is associated with the jet sheath and whether the disk and jet have different proton-to-electron temperature ratios. A space-VLBI array would provide greater clarity than is available from ground-based VLBI alone (Fig. 4).

#### 4.3. AGN jet collimation and variability

Higher-resolution, higher-fidelity imaging would also be a boon to studies of AGN on spatial scales much greater

than  $r_g$ . In the last decade, multiwavelength observations of AGN have been a subject of active investigation. In particular, after the launch of the Fermi telescope and the advent of ground Cherenkov telescopes (e.g., HESS, MAGIC, and VERITAS), VLBI has played an important role in locating the flaring counterpart of high-energy emission (Marscher et al., 2008). High angular resolution observations at millimeter VLBI wavelengths have been useful for constraining properties of the flaring region such as the source size (Akiyama et al., 2015). In the context of multi-messenger observations, resolving the detailed structure of jets will be increasingly important in the next decades, including next-generation Cherenkov telescopes and neutrino observatories.

Increased resolution would also allow AGN jet profiles to be traced closer to the black hole. While radio galaxies often exhibit parabolic collimation profiles near the black hole and a transition to a more conical profile outside (Asada and Nakamura, 2012; Nagai et al., 2014; Boccardi et al., 2016; Tseng et al., 2016; Giovannini et al., 2018; Hada et al., 2018; Nakahara et al., 2018), quasar jet properties are less well studied. A study of the 3C 273 jet is suggestive of a similar transition near its Bondi radius, possibly indicating that jet collimation processes are universal (Akiyama et al., 2018). It has been difficult to obtain enough data to test this hypothesis due to a lack of sufficient resolution. Fig. 5 illustrates that a full space-VLBI array may be necessary to accurately determine jet collimation, with lower-resolution arrays possibly providing an incorrect qualitative understanding of the collimation near the core.

## 5. Discussion

In this work, we have explored a space-VLBI concept that includes space-ground baselines. Such an array can provide fast and/or dense  $(u, v)$  coverage with only a few

<sup>5</sup> The very bright source Cen A may also be on this list, although the black hole mass estimate from stellar kinematics is less encouraging (Cappellari et al., 2009).

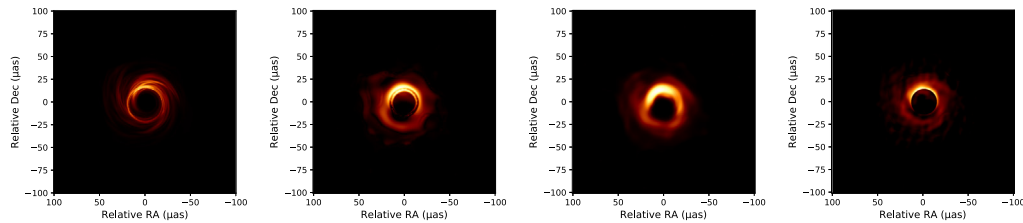


Fig. 4. *Left to right*: Model of the M87 accretion disk and jet (Mościbrodzka et al., 2016, 2017) along with reconstructions of simulated data from the ground-only, ground + LEO, and full space-VLBI array. The helical structure, which is barely resolved with LEO satellites, is clearly visible when MEO/GEO satellites are included.

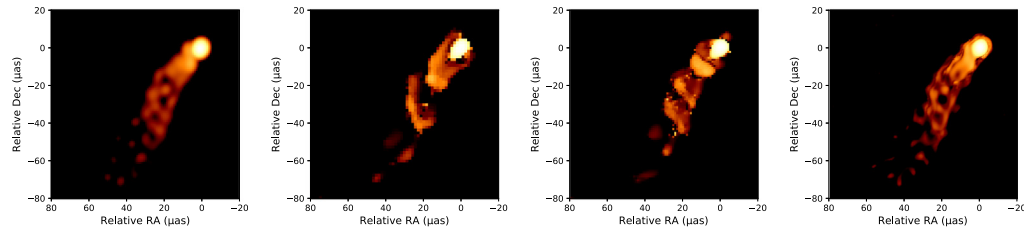


Fig. 5. *Left to right*: Model of the Mrk 501 jet based on rescaling the MOJAVE (Monitoring Of Jets in Active galactic nuclei with VLBA Experiments) 15 GHz image (Lister et al., 2018) along with reconstructions of simulated data from the ground-only, ground + LEO, and full space-VLBI array. The increased resolution of the full space array is required to provide a much truer reconstruction of the details of the jet, including the narrow opening angle by the core, the limb-brightening of the jet, and faint substructures within the jet. A logarithmic transfer function, with the color range spanning three orders of magnitude in dynamic range, is used to highlight weak features in the jet. (For interpretation of the references to colour in this figure legend, the reader is referred to the web version of this article.)

orbiters. Large apertures on the ground provide a cost-effective way to maximize sensitivity. Our simulations demonstrate that a modest space-VLBI array is sufficient to make significant breakthroughs, including measuring the shadows of a larger sample of supermassive black holes, providing detailed images of the jet launch region in M87, and resolving the collimation profiles of a larger collection of AGN jet sources near the black hole.

While many architectural decisions for a space-VLBI concept can be postponed, the question of whether to include space-ground baselines or rely upon only space-space baselines is fundamental and must be decided early. Bringing the data back to the ground has some key advantages, including much faster  $(u, v)$  coverage, better sensitivity, and greater robustness in fringe finding, since a correlator on the ground can more easily handle uncertainties in spacecraft orbits and local-oscillator frequencies/timing. An underappreciated advantage of building space-ground VLBI into the architecture is extensibility. For instance, a pair of telescopes that are in identical orbits but for a small vertical offset, as in the Event Horizon Imager (EHI) concept (Roelofs et al., submitted for publication) could easily be accommodated in a space-ground architecture by the simple addition of a second satellite in MEO. The reverse statement is not true; it would be extremely difficult, if not impossible, to incorporate a number of additional satellites (and ground stations) into the EHI architecture.

For the purposes of this study, we have limited consideration to only the 230 GHz (1.3 mm) band. Nevertheless, as is clear from many of the other articles in this issue, there

is a strong scientific case for including other frequency bands, especially at longer wavelength. Indeed, some aspects of the science in this work (e.g., jet collimation studies) would benefit also benefit from higher-resolution, multiwavelength observations at centimeter and millimeter wavelengths. Having multiple observing bands on VLBI satellites is a cost-effective way to increase the science per dollar as well as the observing duty cycle, since weather conditions will not always be suitable for 230 GHz observing from the ground.

This material is based upon work supported by the National Science Foundation (NSF) under Grant Nos. AST-1440254, AST-1614868, and AST-1659420. M.S. acknowledges support from the NSF Research Experiences for Undergraduates program. K. A. acknowledges support from the Jansky Fellowship of the National Radio Astronomy Observatory (NRAO), a facility of the NSF operated by Associated Universities, Inc. This research has made use of data from the MOJAVE database that is maintained by the MOJAVE team (Lister et al., 2018). We thank Michael Hecht for valuable discussions regarding the technical landscape of satellite systems and Daniel Palumbo for discussions relating to space-VLBI concepts with a small number of antennas in LEO.

*Software*: ehtim (<https://achael.github.io/eht-imaging>), SMILI (<https://github.com/astrosmili/smili>)

## References

- Akiyama, A., Asada, K., Fish, V., Nakamura, M., Hada, K., Nagai, H., Lonsdale, C., 2018. The global jet structure of the archetypical quasar 3C 273. *Galaxies* 6, 15.

- Akiyama, K., Ikeda, S., Pleau, M., et al., 2017a. Superresolution full-polarimetric Imaging for Radio Interferometry with Sparse Modeling. *AJ* 153, 159.
- Akiyama, K., Kuramochi, K., Ikeda, S., et al., 2017b. Imaging the Schwarzschild-radius-scale structure of M87 with the event horizon telescope using sparse modeling. *ApJ* 838, 1.
- Akiyama, K., Lu, R.-S., Fish, V.L., et al., 2015. 230 GHz VLBI observations of M87: event-horizon-scale structure during an enhanced very-high-energy  $\gamma$ -ray state in 2012. *ApJ* 807, 150.
- Asada, K., Nakamura, M., 2012. The structure of the M87 jet: a transition from parabolic to conical streamlines. *ApJ Lett.* 745, L28.
- Broderick, A.E., Loeb, A., 2009. Imaging the black hole silhouette of M87: implications for jet formation and black hole spin. *ApJ* 697, 1164–1179.
- Boccardi, B., Krichbaum, T.P., Bach, U., Mertens, F., Ros, E., Alef, W., Zensus, J.A., 2016. The stratified two-sided jet of Cygnus A. *Acceleration and collimation. A&A* 585, A33.
- Bouman, K.L., Johnson, M.D., Zoran, D., Fish, V.L., Doeleman, S.S., Freeman, W.T., 2016. Computational imaging for VLBI image reconstruction. In: *IEEE Conf. on Computer Vision and Pattern Recognition*, Seattle, WA, USA, 27–30 June 2016.
- Cappellari, M., Neumayer, N., Reunanen, J., van der Werf, P.P., de Zeeuw, P.T., Rix, H.-W., 2009. The mass of the black hole in Centaurus A from SINFONI AO-assisted integral-field observations of stellar kinematics. *MNRAS* 394, 660–674.
- Chael, A.A., Johnson, M.D., Narayan, R., Doeleman, S.S., Wardle, J.F.C., Bouman, K.L., 2016. High-resolution linear polarimetric imaging for the event horizon telescope. *ApJ* 829, 11.
- Cohen, M.H., Kellermann, K.I., Shaffer, D.B., et al., 1977. Radio sources with superluminal velocities. *Nature* 268, 405–409.
- Dexter, J., McKinney, J.C., Agol, E., 2012. The size of the jet launching region in M87. *MNRAS* 421, 1517–1528.
- Doeleman, S.S., Fish, V.L., Schenck, D.E., et al., 2012. Jet-launching structure resolved near the supermassive black hole in M87. *Science* 338, 355–358.
- Fish, V., Alef, W., Anderson, J., et al., 2013. High-angular-resolution and high-sensitivity science enabled by beamformed ALMA, arXiv:1309.3519>.
- Gebhardt, K., Adams, J., Richstone, D., Lauer, T.R., Faber, S.M., Gültekin, K., Murphy, J., Tremaine, S., 2011. The black hole mass in M87 from Gemini/NIFS adaptive optics observations. *ApJ* 729, 119.
- Giovannini, G., Savolainen, T., Orienti, M., et al., 2018. A wide and collimated radio jet in 3C84 on the scale of a few hundred gravitational radii. *Nat. Astron.* 2, 472–477.
- Gómez, J.L., Lobanov, A.P., Bruni, G., et al., 2016. Probing the innermost regions of AGN jets and their magnetic fields with RadioAstron. I. Imaging BL Lacertae at 21 microarcsecond resolution. *ApJ* 817, 96.
- Greene, J.E., Seth, A., Kim, M., et al., 2016. Megamaser disks reveal a broad distribution of black hole mass in spiral galaxies. *ApJ Lett.* 826, L32.
- Hada, K., Doi, A., Nagai, H., Inoue, M., Honma, M., Giroletti, M., Giovannini, G., 2013. Evidence of a nuclear radio jet and its structure down to  $\lesssim 100$  Schwarzschild Radii in the center of the sombrero galaxy (M 104, NGC 4594). *ApJ* 779, 6.
- Hada, K., Doi, A., Wajima, K., D’Ammando, F., Orienti, M., Giroletti, M., Giovannini, G., Nakamura, M., Asada, K., 2018. Collimation, acceleration, and recollimation shock in the jet of gamma-ray emitting radio-loud narrow-line Seyfert 1 Galaxy 1H0323+342. *ApJ* 860, 141.
- Hirabayashi, H., Hirosawa, H., Kobayashi, H., et al., 1998. Overview and initial results of the very long baseline interferometry space observatory programme. *Science* 281, 1825–1829.
- Hong, X., Shen, Z., An, T., Liu, Q., 2014. The Chinese space millimeter-wavelength VLBI array—A step toward imaging the most compact astronomical objects. *Acta Astronaut.* 102, 217–225.
- Johnson, M.D., Fish, V.L., Doeleman, S.S., et al., 2015. Resolved magnetic-field structure and variability near the event horizon of Sagittarius A\*. *Science* 350, 1242–1245.
- Johannsen, T., Psaltis, D., Gillessen, S., Marrone, D.P., Özel, F., Doeleman, S.S., Fish, V.L., 2012. Masses of nearby supermassive black holes with very long baseline interferometry. *ApJ* 758, 30.
- Kardashev, N.S., Khartov, V.V., Abramov, V.V., et al., 2013. “Radio-Astron”—A telescope with a size of 300 000 km: main parameters and first observational results. *Astron. Rep.* 57, 153–194.
- Kellermann, K.I., Clark, B.G., Shaffer, D.B., Cohen, M.H., Jauncey, D. L., Broderick, J.J., Niell, A.E., 1974. Further observations of apparent changes in the structure of 3c 273 and 3c 279. *ApJ Lett.* 189, L19–L22.
- Kuramochi, K., Akiyama, K., Ikeda, S., Tazaki, F., Fish, V.L., Pu, H.-Y., Asada, K., Honma, K., 2018. Superresolution interferometric imaging with sparse modeling using total squared variation: application to imaging the black hole shadow. *ApJ* 858, 56.
- Levy, G.S., Linfield, R.P., Ulvestad, J.S., et al., 1986. Very long baseline interferometric observations made with an orbiting radio telescope. *Science* 234, 187–189.
- Lister, M.L., Aller, M.F., Aller, H.D., Hodge, M.A., Homan, D.C., Kovalev, Y.Y., Pushkarev, A.B., Savolainen, T., 2018. MOJAVE. XV. VLBA 15 GHz total intensity and polarization maps of 437 parsec-scale AGN jets from 1996 to 2017. *ApJS* 234, 12.
- Lu, R.-S., Fish, V.L., Akiyama, K., et al., 2013. Fine-scale structure of the Quasar 3C 279 measured with 1.3 mm very long baseline interferometry. *ApJ* 772, 13.
- Marrone, D.P., Moran, J.M., Zhao, J.-H., Rao, R., 2007. *ApJ Lett.* 654, L57–L60.
- Marrone, D.P., Baganoff, F.K., Morris, M.R., et al., 2008. An X-ray, infrared, and submillimeter flare of Sagittarius A\*. *ApJ* 682, 373–383.
- Marscher, A.P., Jorstad, S.G., D’Arcangelo, F.D., et al., 2008. The inner jet of an active galactic nucleus as revealed by a radio-to- $\gamma$ -ray outburst. *Nature* 452, 966–969.
- Mościbrodzka, M., Dexter, J., Davelaar, J., Falcke, H., 2017. Faraday rotation in GRMHD simulations of the jet launching zone of M87. *MNRAS* 468, 2214–2221.
- Mościbrodzka, M., Falcke, H., Shiokawa, H., 2016. General relativistic magnetohydrodynamical simulations of the jet in M87. *A&A* 586, A38.
- Murphy, D., Preston, R., Fomalont, E., Romney, J., Ulvestad, J., Greenhill, L., Reid, M., 2005. iARISE: A next-generation two-spacecraft space VLBI mission concept. *ASPC* 340, 575–577.
- Nagai, H., Haga, T., Giovannini, G., et al., 2014. Limb-brightened jet of 3C 84 revealed by the 43 GHz very-long-baseline-array observation. *ApJ* 785, 53.
- Nakahara, S., Doi, A., Murata, Y., Hada, K., Nakamura, M., Asada, K., 2018. Finding transitions of physical condition in jets from observations over the range of  $10^3$ – $10^9$  Schwarzschild Radii in radio Galaxy NGC 4261. *ApJ* 854, 148.
- Palumbo, D., 2018. Expanding the Event Horizon Telescope to Space: a Conceptual Study, presentation at The Future of High-Resolution Radio Interferometry in Space, Noordwijk, The Netherlands, 2018 September 5–6, <[https://www.ru.nl/publish/pages/903733/palumbo\\_eht\\_svlbi.pdf](https://www.ru.nl/publish/pages/903733/palumbo_eht_svlbi.pdf)>.
- Palumbo, D., Johnson, M., Doeleman, S., Chael, A., Bouman, K., 2018. Next-generation Event Horizon Telescope developments: new stations for enhanced imaging. *AAS* 231, 347.21.
- Primiani, R.A., Young, K.H., Young, A., Patel, N., Wilson, R.W., Vertatschitsch, L., Chitwood, B.B., Srinivasan, R., MacMahon, D., Weintraub, J., 2016. SWARM: a 32 GHz correlator and VLBI beamformer for the submillimeter array. *J. Astronom. Instrum.* 5, 1641006.
- Roelofs, R., Falcke, H., Brinkerink, C., et al., eIofs et al., submitted for publication. On the prospects of imaging the event horizon of Sagittarius A\* from space. *A&A*, submitted for publication.
- Tseng, C.-Y., Asada, K., Nakamura, M., Pu, H.-Y., Algaba, J.-C., Lo, W.-P., 2016. Structural transition in the NGC 6251 jet: an interplay with the supermassive black hole and its host galaxy. *ApJ* 833, 288.
- Walker, R.C., Hardee, P.E., Davies, F.B., Ly, C., Junor, W., 2018. The structure and dynamics of the Subparsec Jet in M87 based on 50 VLBA observations over 17 Years at 43 GHz. *ApJ* 855, 128.

Warmels, R., Biffs, A., Cortes, P.A., et al. 2018, ALMA Technical Handbook, ALMA Doc 6.3, ver 1.0, <<https://almascience.nrao.edu/documents-and-tools/cycle6/alma-technical-handbook>>.

Whitney, A.R., Shapiro, I.I., Rogers, A.E.E., Robertson, D.S., Knight, C. A., Clark, T.A., Goldstein, R.M., Marandino, G.E., Vandenberg, N. R., 1971. Quasars revisited: rapid time variations observed via very-long-baseline interferometry. *Science* 173, 225–230.